Commercial Sensor Survey Radiation Testing Progress Report

Heidi N. Becker
Michael D. Dolphin
Dennis O. Thorbourn
James W. Alexander
Phil M. Salomon

Jet Propulsion Laboratory
Pasadena, California

Commercial Sensor Survey Testing Progress Report

NASA Electronic Parts and Packaging (NEPP) Program
Office of Safety and Mission Assurance

Heidi N. Becker
Michael D. Dolphin
Dennis O. Thorbourn
James W. Alexander
Phil M. Salomon

Jet Propulsion Laboratory
Pasadena, California

NASA WBS: 939904.01.11.30
JPL Project Number: 102197
Task Number: 3.21.4

Jet Propulsion Laboratory
4800 Oak Grove Drive
Pasadena, CA 91109

http://nepp.nasa.gov

Table of Contents

Acronym List

ADC   Analog-to-Ditigal Converter
CMOS   Complementary Metal Oxide Semiconductor
DDD   Displacement Damage Dose
DN   Digital Number (analog-to-digital converter count)
DSNU   [Pixel] Dark Signal Non-Uniformity
LED   Light Emitting Diode
OV   OmniVision
MOSFET   Metal Oxide Semiconductor Field Effect Transistor
NEPP   NASA Electronic Parts and Packaging (Program)
PRNU   [Pixel] Photo Response Non-Uniformity
RTS   Random Telegraph Signal
TID   Total Ionizing Dose
USAF   United States Air Force

1.0   Introduction

The NASA Electronic Parts and Packaging (NEPP) Program Sensor Technology Commercial Sensor Survey task is geared toward benefiting future NASA space missions with low-cost, short-duty-cycle, visible imaging needs. Such applications could include imaging for educational outreach purposes or short surveys of spacecraft, planetary, or lunar surfaces. Under the task, inexpensive commercial grade CMOS sensors were surveyed in fiscal year 2007 (FY07) and three sensors were selected for total ionizing dose (TID) and displacement damage dose (DDD) tolerance testing. The selected sensors had to meet selection criteria chosen to support small, low-mass cameras that produce good resolution color images. These criteria are discussed in detail in [1]. This document discusses the progress of radiation testing on the Micron and OmniVision sensors selected in FY07 for radiation tolerance testing.

2.0   Sensors Selected for Radiation Testing

Following are brief descriptions of the selected sensors and the manufacturer-supplied evaluation kits used for our characterizations. Details of evaluation kit support software are proprietary to Micron and OmniVision and are not discussed in this document.

2.1   Micron

2.1.1   Micron MT9P031 (5 Mpixel, 1/2.5 inch, 2.2 µm) – "Micron 5MPX"

The MT9P031 is a 5-Mpixel, 1/2.5-inch optical format, CMOS sensor with a 2592(H) × 1944(V) color pixel array that employs a red-green-blue (RGB) Bayer pattern color filter. The pixel size is 2.2 µm × 2.2 µm. This product is marketed for applications that include high-resolution network cameras, wide field-of-view cameras, and hybrid video cameras with high resolution stills. Among its features are a 12-bit, on-chip analog-to-digital converter (ADC); 381-mW power consumption when imaging at full resolution and 14 frames-per-second; and low dark current and read noise [2].

2.1.2   Micron MT9T031 (3.1 Mpixel, 1/2 inch, 3.2 µm) – "Micron 3MPX"

The MT9T031 is a 3.1-Mpixel, 1/2-inch CMOS sensor with a 2048(H) × 1536(V) pixel array and RGB Bayer pattern color filter. The pixel size is 3.2 µm × 3.2 µm. This sensor has a 10-bit, on-chip ADC; 228-mW power consumption when imaging at full resolution and 12 frames per second; and low dark current and read noise. This sensor is also marketed for wide field-of-view cameras, video cameras, and high resolution stills [3].

2.1.3   Micron Evaluation Kit

Evaluation of both Micron sensors was supported by Micron's Demo2 Evaluation Hardware Kit (Figure 1) and accompanying DevWare software. This kit uses

interchangeable camera headboards that are customized for each sensor product. The headboards for the Micron 5MPX and 3MPX were modified to include a test sample socket integrated with the camera's optical barrel. This modification allowed many sensor samples to be evaluated using the same headboard electronics. The custom sockets were designed with a thermocouple access point to allow temperature monitoring of samples during characterization.
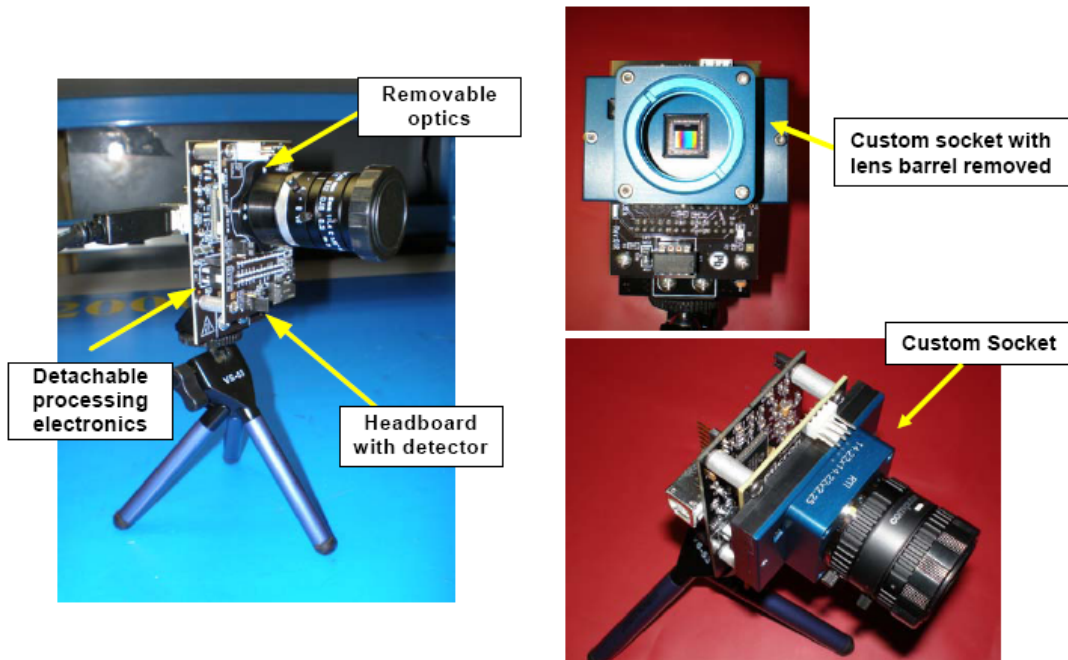
Fig. 1. Micron CMOS sensor evaluation camera with custom socket

2.2 OmniVision

2.2.1 OV3630 (3.2 Mpixel, 1/3.2 inch, 2.2 µm)

The OV3630 is a 3.2-Mpixel, 2.2 µm × 2.2 µm pixel, 1/3.2-inch CMOS CameraChip^{TM}. This sensor has an on-chip, 10-bit ADC and can operate up to 15 frames per second at full resolution. It operates in both video and snapshot mode and is marketed for digital still image and video/still camera products. Power consumption is <110 mW (active) [4]. OmniVision's ECX evaluation module [5] is designed with a detachable prototyping module (headboard), which contains a solder-mounted sensor sample and removable optics (Figure 2). The design allows test samples to be irradiated without removing them from the camera headboards or harming any support electronics (optics were removed for irradiation). Test samples for the OV3630 were procured as individual evaluation modules.

2
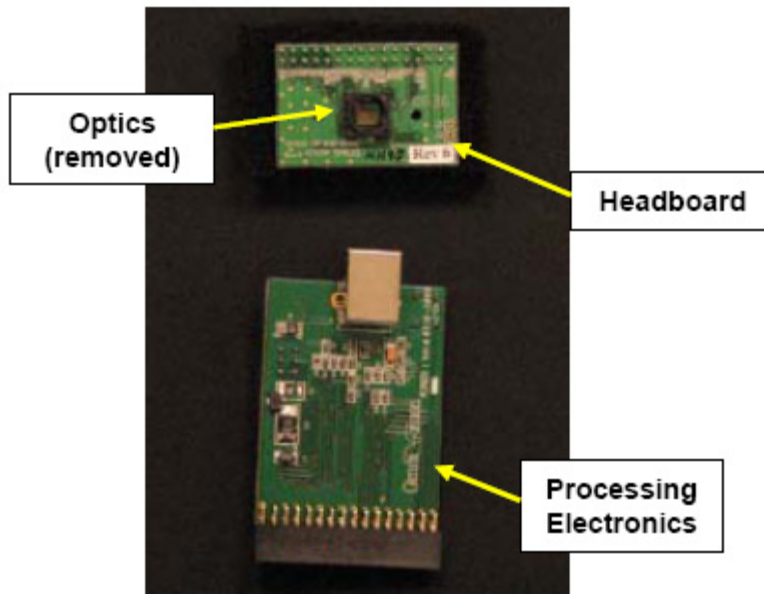
Fig. 2. OV3530 ECX Evaluation Module

3.0   Test Bench

The Commercial Sensor Survey test bench (Figure 3) has a shrouded black box that can be used for collecting dark frames or imaging. Internal equipment includes a neutral white LED light source and an integrating sphere for flat field illumination, a USAF bar target for imaging, and thermocouples for monitoring ambient temperature and sensor sample temperature (Micron). The optical barrel of the OmniVision (OV) evaluation module does not allow easy access to the sensor sample inside, so OV3630 proximity board temperature, rather than sample temperature, was monitored. Sensor register settings and data collection are controlled via a laptop interface.

Fig. 3. Commercial Sensor Survey Test Bench

4.0   Characterization Approach

4.1   Manual and Auto

All three sensors are designed with on-chip image correction features to provide low noise performance (e.g., black-level calibration, analog and digital offset corrections, etc.). However, the function of these features is to subtract o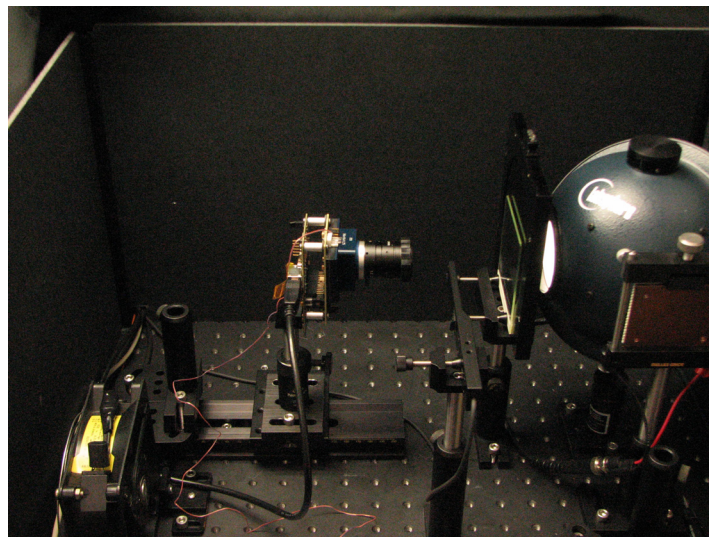r adjust for device parameters that can change following radiation exposure. A good example is the correction of pixel dark signal, the rates of which increase with total ionizing dose (TID) and displacement damage dose (DDD). In order to identify the uncorrected radiation degradation in basic device parameters, and also to see how these effects could be corrected via on-chip image correction features, our approach to characterizing the radiation response of the three sensor technologies had two components:

1)   Manual: Data collection with sensor register settings adjusted to control parameters that can influence characterization results:

   a)   Use of fixed exposure times, manual offset selection, and fixed internal signal chain gains (analog and digital), to ensure integrity of all pixel data without pixel or ADC saturation.
   b)   Disabled on-chip image correction features (such as black-level calibration/correction, noise reduction, and white balance) for accurate determination of dark signal rates, pixel noise, and photoresponse.

2)   Auto: Data collection with sensor auto functions enabled to see how radiation degradation effects are corrected internally by the sensor.

Note that in a camera application, the camera designer would likely choose some combination of manually controlled and auto-controlled register settings, depending on the particular imaging need. For our data collection, default evaluation kit auto settings were used.

4.2   Data Sets

The following data sets were collected pre- and post-irradiation:

1)   Manual:

   a)   Dark frames collected at several different integration times (used for pixel dark signal rate, noise, and dark signal non-uniformity [DSNU] calculations)
   b)   Flat field images at several different integration times (used for photon transfer curves, noise, and photo response non-uniformity [PRNU] calculations)
   c)   Bar target images taken at best focus for different integration times (used for qualitative imaging assessment). One set of images was collected at the

exposure time; gain settings were chosen by the sensor during auto bar target image collection.

2) Auto:

    a) Dark frames (at one auto exposure time chosen by the sensor; black-level calibration/correction and white balance enabled; gains automatically chosen by the sensor)

    b) Flat field images (at one auto exposure time chosen by the sensor)

    c) Bar target images taken at best focus (used for qualitative imaging assessment)

Each data set included five frames taken under identical conditions in rapid succession. Optically black reference pixel values were saved for every manual and auto data frame. All data were collected at ambient temperature.

4.3   Analyzed Sensor Parameters

Mean Dark Signal Rate: The average pixel signal rate under un-illuminated conditions.

Local Pixel DSNU: The average rms value of pixel dark signal calculated over local 16 x 16 pixel windows. In our calculations, local DSNU was calculated on a color-wise basis (e.g., local DSNU calculated for only green1 pixels, red pixels, blue pixels, or green2 pixels) to remove the effects of any offsets between the four colors.

Pixel PRNU: The rms value of pixel photo response under flat field (uniform) illumination conditions.

Pixel Noise: The average rms signal value. The calculations in this report were performed using data taken under un-illuminated conditions with various integration times. Pixel noise under these conditions includes a combination of thermal dark current shot noise, output amplifier noise, on-chip electronic noise, and any uncorrected offset noise or pixel reset noise.

Gain: CMOS sensor (camera) gain in signal electrons/ADC unit (e/DN).

5.0   Radiation Test Levels

Our radiation test levels were based on a range of displacement damage dose (DDD) and total ionizing dose (TID) levels that are considered typical for outreach or survey cameras in Earth orbit or Deep Space solar flare environments (e.g., Mars). These types of cameras typically have to compete with other payloads and flight system instruments which may have higher priority for available shielding mass and strategic positioning on the spacecraft. The negotiated amount of shielding would depend on the priority of the camera's data return, how early in the mission the camera would be expected to achieve

its requirements, the relative radiation sensitivity of the sensor technology, and the risk to meeting performance requirements due to radiation degradation or transient noise.

In the environments considered, high energy protons are the dominant contributors to cumulative mission DDD and TID. 50-MeV protons were selected for our irradiations because this energy is representative of the typical radiation spectrum at the detector level, after having passed through instrument shielding. This allowed us to perform representative TID and DDD testing simultaneously. The radiation test levels listed in Table 1 show target TID levels and the corresponding 50-MeV proton test fluence and DDD in silicon.

Table 1. Radiation Test Levels

Total Ionizing Dose (TID) rad(Si)	50-MeV† Proton Test Fluence (protons/cm^2)	Displacement Damage Dose (MeV/g)*
500	3.16E9	1.2E7**
1000	6.32E9	2.4E7
2000	1.26E10	4.9E7
5000	3.16E10	1.2E8***

*DDD was calculated using the following relationship:
> **DDD (MeV/g) = test particle NIEL (MeV·cm^2/g) × test particle fluence (particles/cm^2)**
> [calculations performed using 3.884E-3 MeV*cm^2/g Si(21eV) NIEL value for 50-MeV protons from Summers et. al, *IEEE Trans. Nucl. Sci.*, 40(6), Dec. 1993]

**Considered a lower bound, below which significant shielding would be required
***Considered a representative upper bound
†It was not possible to procure our test samples with removable cover glass, so irradiations had to be performed through the sensor cover glass. Proton energy loss calculations for incident 51-MeV protons (used for all irradiations) were performed using manufacturer-supplied information on cover glass thickness and material. For all three sensors, the energy loss was ~1-MeV, and the proton energy incident on the sensor die was 50-MeV.

Preliminary radiation testing was performed in the first quarter of fiscal 2008 (1Q08). TID testing was performed at the Jet Propulsion Laboratory's (JPL's) Co-60 ionizing dose facility on the OV and Micron sensors, and combined TID/DDD testing was performed on the Micron sensors with 50-MeV protons at the University of California (UC) Davis cyclotron. These experiments served as pathfinder tests, which revealed the need for various test protocol changes and sensor register setting revisions to sufficiently suppress auto correction features and to ensure fidelity and desired resolution of all pixel data.

The data presented in this Testing Progress Report were taken following 50-MeV proton irradiations at UC Davis in February 2008. For each sensor technology (OV, Micron 3MPX, Micron 5MPX), four samples were irradiated. Each of the four samples was exposed to one of the radiation test levels listed in Table 1 (Figure 4) and returned to JPL for characterization; no incremental dose testing or on-site characterization at UC Davis was performed. This decision was made to ensure that data collection could be repeated, if necessary, to fill any gaps in the data sets (i.e., saturated pixels, low signal resolution, etc.), and also to avoid the complication of spurious signal due to sample activation.
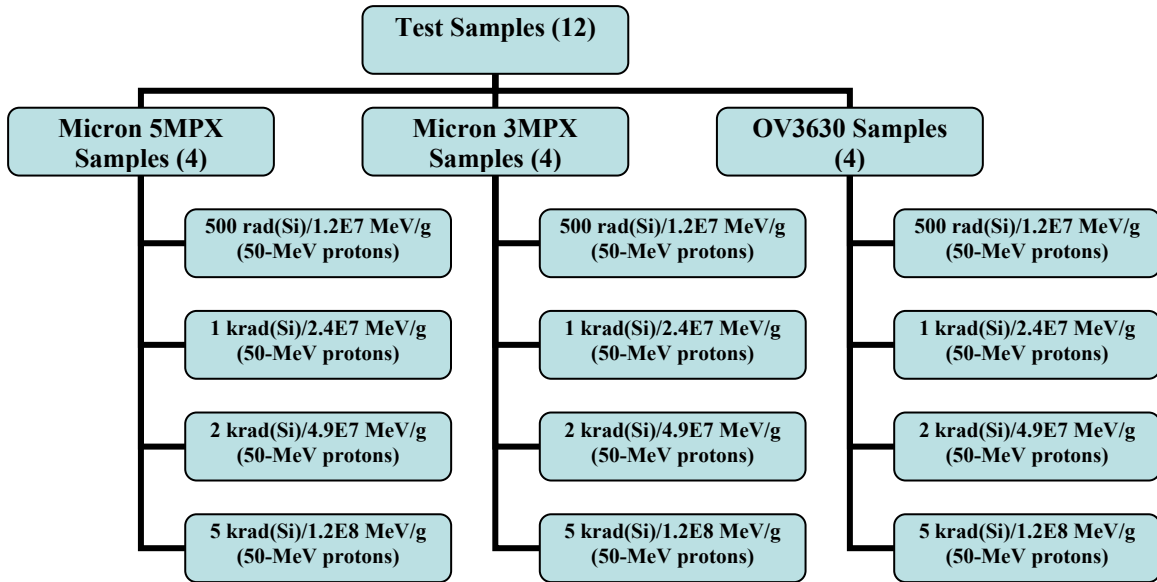
Fig. 4. Radiation Test Sample Allocation

6.0 Radiation Test Conditions

Samples were irradiated unpowered with all leads shorted to ground. Unpowered irradiation was chosen for initial testing because it is considered representative of the low-duty cycles of the camera applications addressed by this study. Characterizations were performed within several weeks following irradiation.

7.0 Micron Test Results

7.1 Parametric Characterizations (Manual)

7.1.1 Gain

Data in this report are expressed in terms of digital number (DN) (analog-to-digital converter count). The conversion from DN to electrons can be found by plotting the signal variance (DN^2) vs. average signal level under flat field illumination conditions. For the range of signal levels dominated by shot noise, electron gain is given by the slope of this linear region:

$$e/DN = \frac{\overline{signal}(DN)}{\sigma^2(DN^2)} \qquad (1)$$

An example of this technique is shown in Figure 5 for the Micron 3MPX sensor. Similar calculations were performed to determine e/DN for the Micron 5MPX sensor and the OV3630. Results for all three sensors are shown in Table 2.
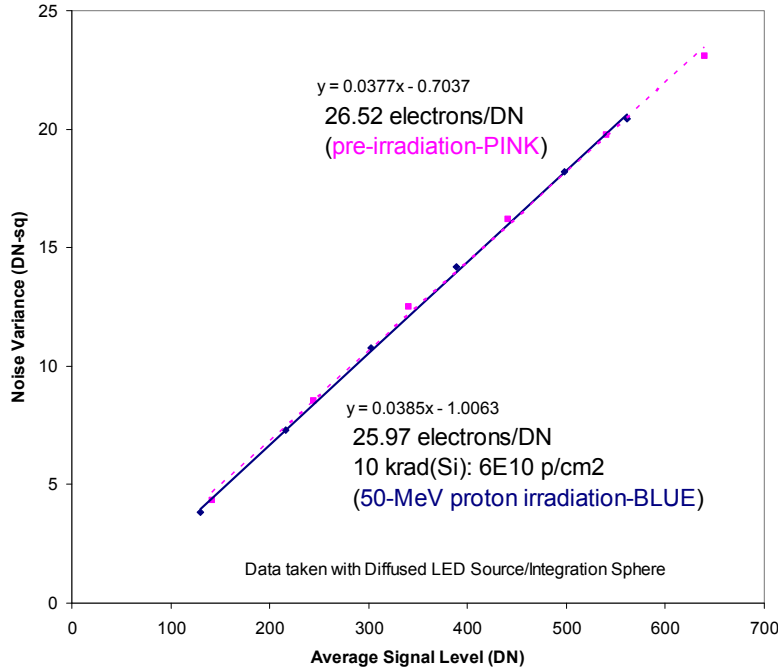

y = 0.0377x - 0.7037
26.52 electrons/DN
(pre-irradiation-PINK)

y = 0.0385x - 1.0063
25.97 electrons/DN
10 krad(Si): 6E10 p/cm2
(50-MeV proton irradiation-BLUE)

Data taken with Diffused LED Source/Integration Sphere

Fig. 5. Photon transfer curves for a 3MPX Micron sensor sample. Our calculated value of ~26 e/DN matches well with the MT9T031 spec value. Virtually no degradation in electronic gain was observed following unbiased irradiation to 10 krad(Si) with 50-MeV protons (data from 1Q08 pathfinder testing).

Table 2. Calculated Electronic Gain (e/DN)

Sensor	Micron 3MPX	Micron 5MPX	OV3630
electrons/DN	26	2.5	55

7.1.2 Dark Signal

Prior to irradiation, dark signal data was collected with integration times ranging from 500 ms to 4 s (3MPX), and 500 ms to 2.5 s (5MPX). A gain of 32 was used for all four color channels (red, green1, blue, green2). The long integration times and relatively high gain setting were required to achieve good resolution of the low pixel dark rates seen prior to irradiation. After irradiation, broad distributions of dark signal values (with many "hot pixels") required that two sets of dark frames be collected to ensure that all pixel values were captured without pixel or ADC saturation. One set was collected with the same gain and range of integration times that was used prior to irradiation. The second set

was collected using a gain of 2 and a reduced range of integration times: 50 ms to 400 ms.

For all pre- and post-irradiation data sets, five frames were taken at each integration time. From each set of five frames, an average frame was calculated on a pixel-by-pixel basis. The mean dark rate was calculated for each pixel position by taking the difference of the average dark signal at two integration times, dividing by the difference in integration time, and normalizing for a gain of 1. In order to calculate the mean dark rate for the entire array, pixel information from the two post-irradiation data sets had to be merged. The majority of pixels had post-irradiation dark rates that were low enough to use the data collected with the longer integration times and higher gain setting, but dark rates for the hotter pixels were calculated using the data collected with lower gain and integration times. Using this approach, the mean dark rate over the entire image was calculated by averaging the mean dark rates of the individual pixels.

Figure 6 shows the increase in mean dark rate as a function of ionizing dose for the Micron 3MPX and 5MPX sensors. Rates are given in DN (ADC count) per pixel per second. See Section 7.1.1 for conversions from DN to electrons for the 3MPX and 5MPX.
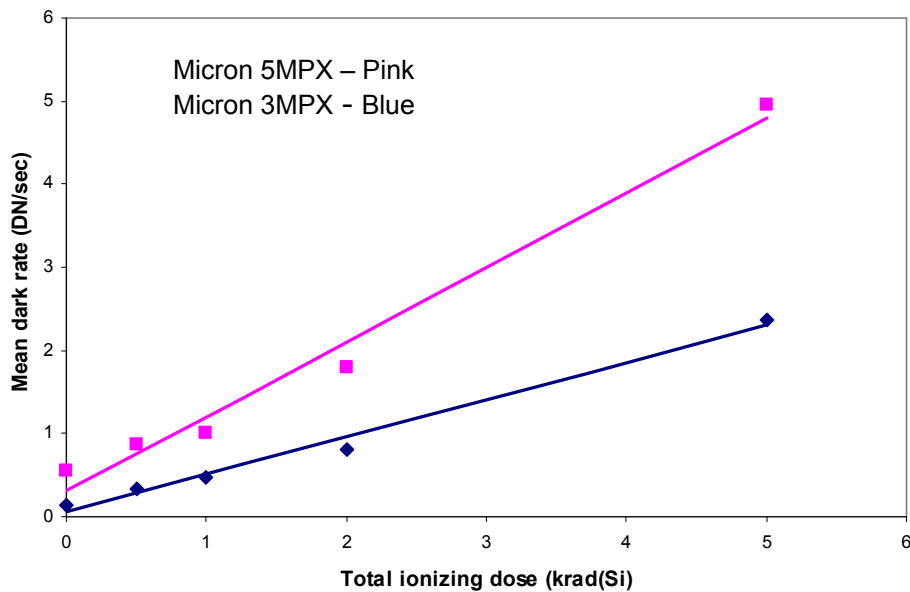

Fig. 6. Mean pixel dark rate vs. ionizing dose for Micron sensors irradiated unbiased with 50-MeV protons. During data collection, sensor package temperature was monitored at ~+30°C (3MPX) and ~+31°C (5MPX).

The contribution of hotter pixels in the distributions has a tendency to skew the calculated mean dark rates toward higher values. Median dark rate values (~1/2 as large as the typical mean values) are perhaps a better metric for typical radiation-induced dark rate increases.

Pixel dark rate distributions are shown in Figures 7 and 8. Pre-irradiation distributions for typical samples are included. Following 50-MeV proton irradiation, there is little change to the original dark rate distribution, but a second distribution (or "tail") for higher dark rate pixels begins to emerge. This is especially evident in the 5MPX dark rate distributions shown in Figure 7, where two distinct peaks can be seen in each post-irradiation distribution.
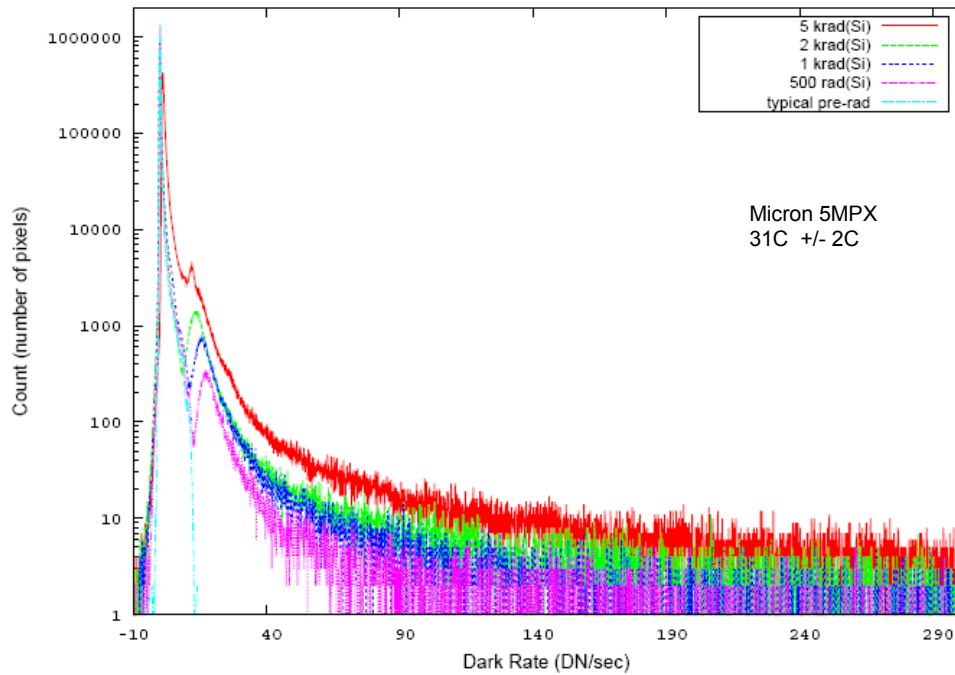

Fig. 7. Dark rate distributions for Micron 5MPX samples irradiated unbiased with 50-MeV protons. A typical pre-irradiation dark rate distribution is included. Data were collected with on-chip image correction functions disabled.

Fig. 8. Dark rate distributions for Micron 3MPX samples irradiated unbiased with 50-MeV protons. A typical pre-irradiation dark rate distribution is included. Data were collected with on-chip image correction functions disabled.
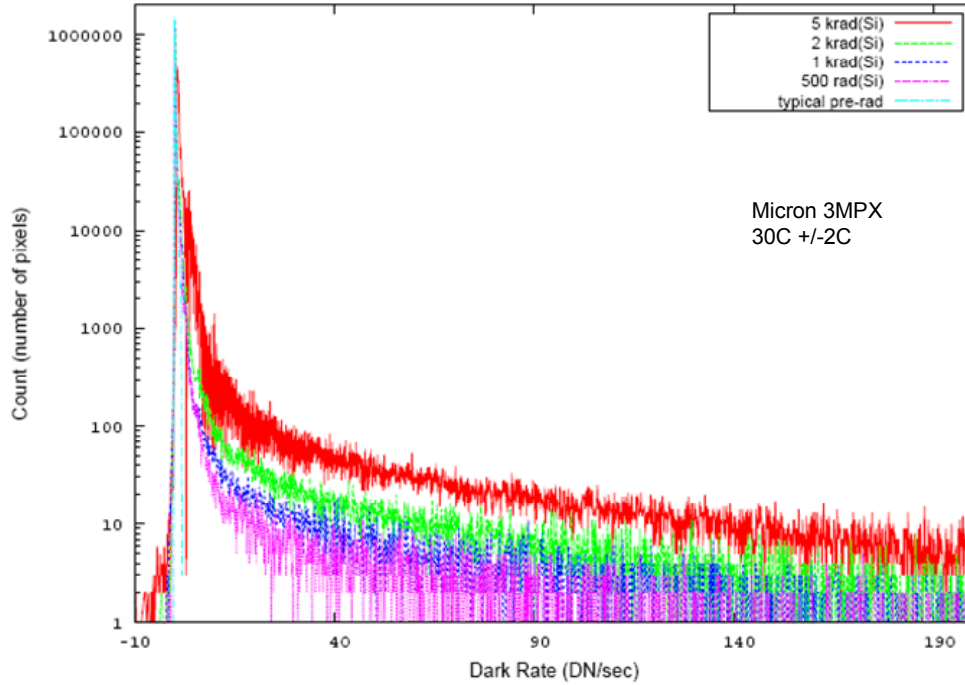
Figures 9 and 10 are semi-log plots of (1 - cumulative distribution function) for pixel dark rates seen after each irradiation level. Pre-irradiation data are also presented for a typical sample. This plotting format allows the percentage of pixels with dark rates greater than a given value to be compared for different irradiation levels. The increased percentage of hotter pixels at the higher irradiation levels is particularly evident in the 5MPX data. For both sensors, the increased numbers of higher dark rate pixels scales with proton fluence.
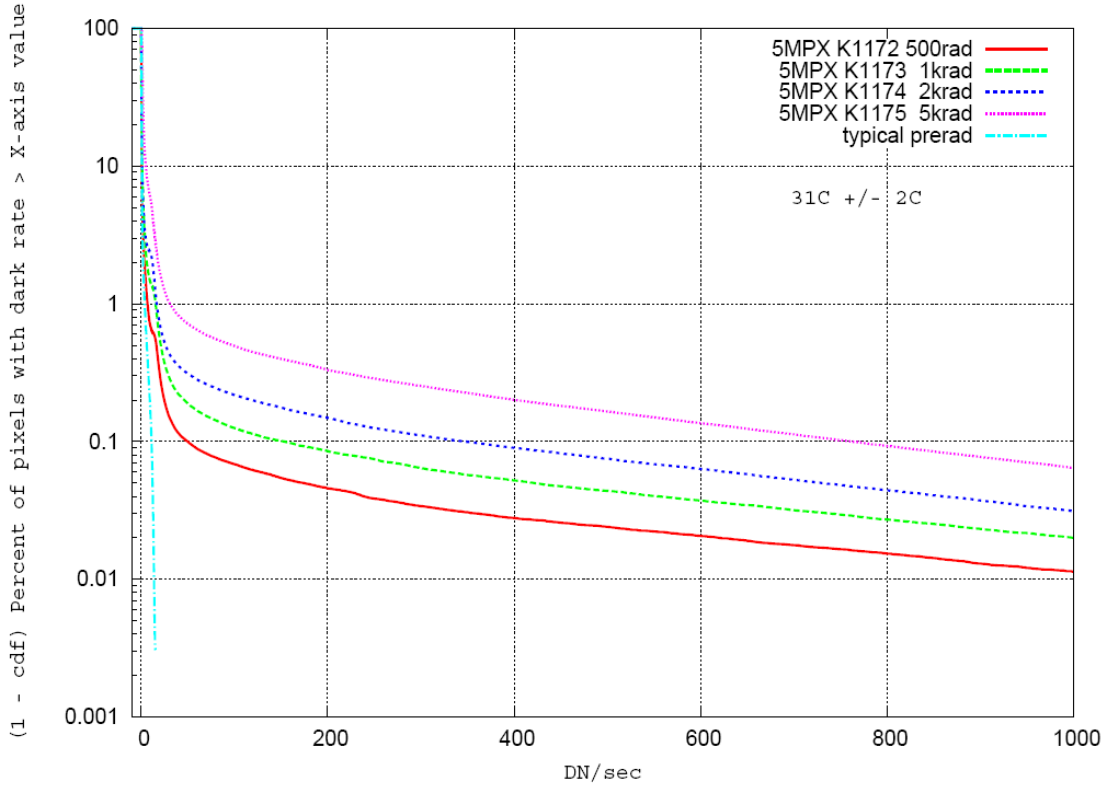
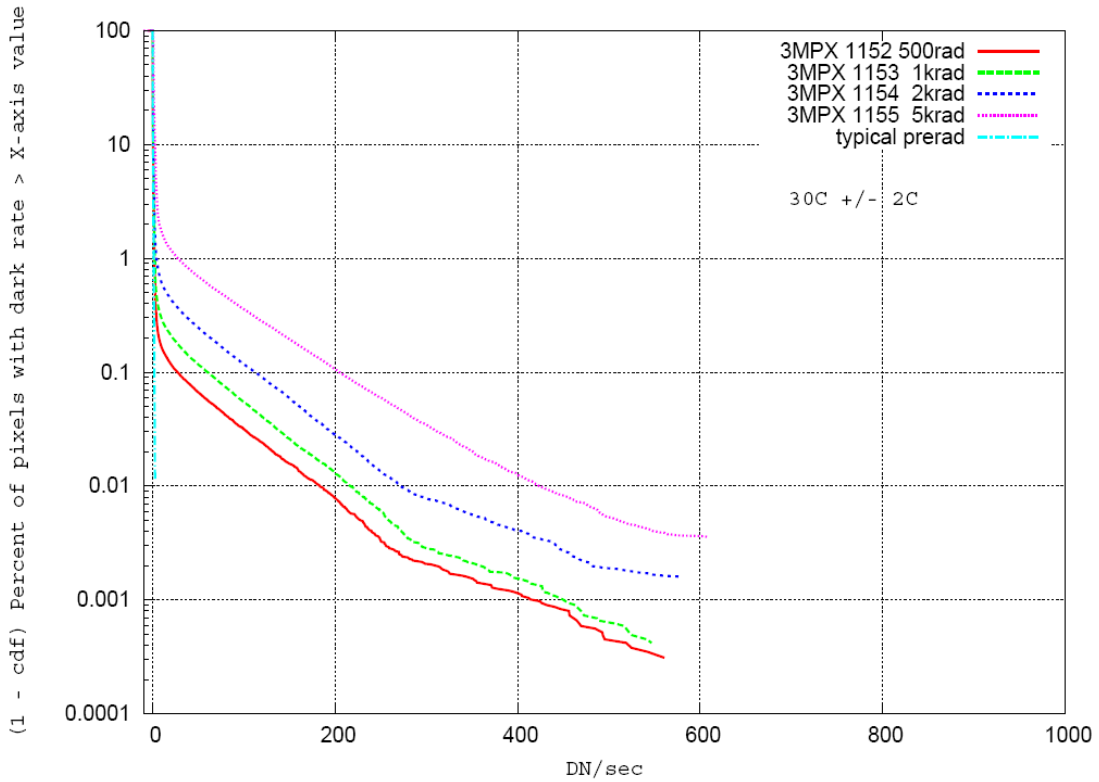**Fig. 9.** Percentage of Micron 5MPX pixels with dark rates above a given rate

Fig. 10. Percentage of Micron 3MPX pixels with dark rates above a given rate

7.1.3   Dark Signal Non-Uniformity (DSNU)

Local DSNU was calculated for green1 pixels by dividing the array into several 16x16 green1 "windows" and calculating the rms dark rate value over each window. The average rms value for all windows (the "Local DSNU") represents the typical DSNU that could impact local image quality. These analysis results are presented below in three different formats to illustrate the increase in DSNU from the pre-irradiation case to each irradiation level (Table 3, Figure 11, Table 4, and Figure 12):

1)   A table of the calculated local DSNU
2)   A 3D plot of the individual 16x16 window rms dark rate values
3)   A 2D surface plot of the window rms values

Table 3. Micron 3MPX Local DSNU.
Local DSNU values (the average rms window values) for each irradiation level.

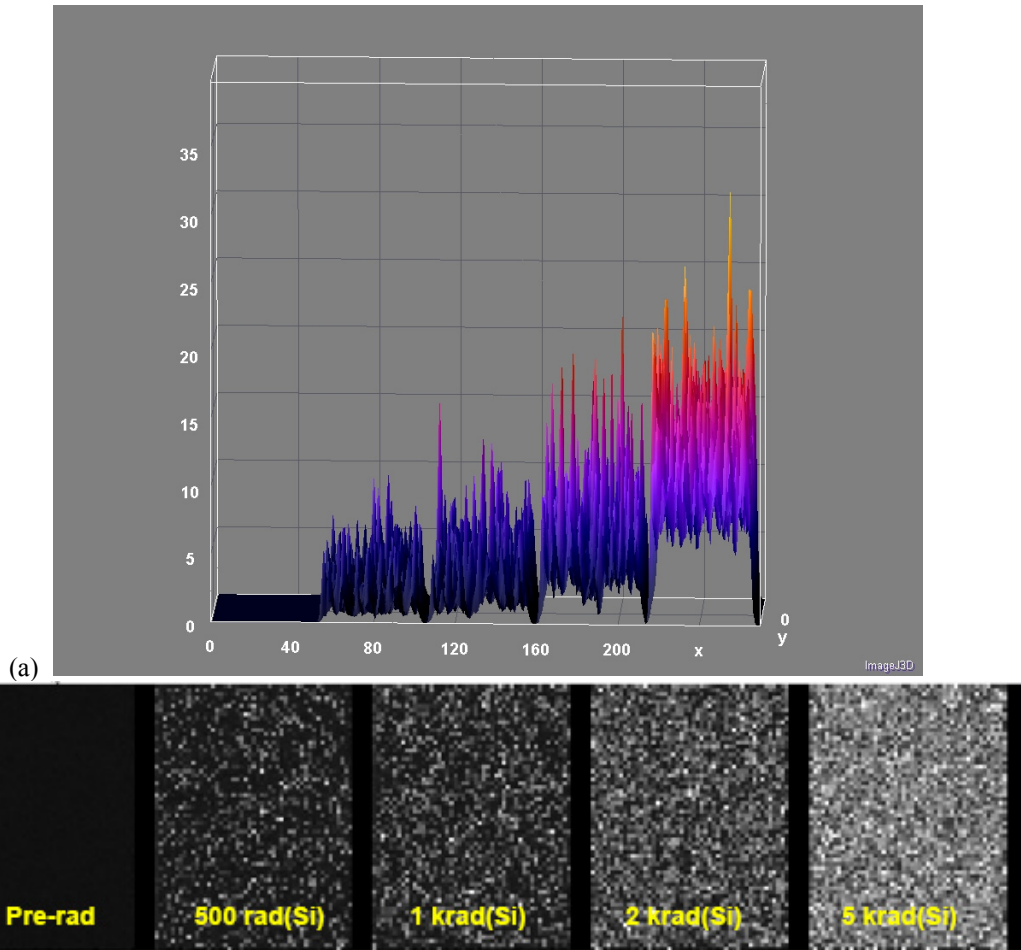| Irradiation Level	Pre-irradiation	500 rad(Si)	1 krad(Si)	2 krad(Si)	5 krad(Si)
Local DSNU (DN)	0.181	1.880	2.798	5.154	10.973

(a)

(b)

Fig. 11. Micron 3MPX Local DSNU. (a) 3D plots of rms dark rate values (in DN) for each 16x16 window of green1 pixels in the Micron 3MPX sensor. Irradiation levels increase from left to right, and pre-irradiation data are shown at the far left. (b) 2D surface plots for all five cases are shown below the 3D plot to further illustrate the variations across the array.

13

Table 4. Micron 5MPX Local DSNU.
Local DSNU values (the average rms window values) for each irradiation level.

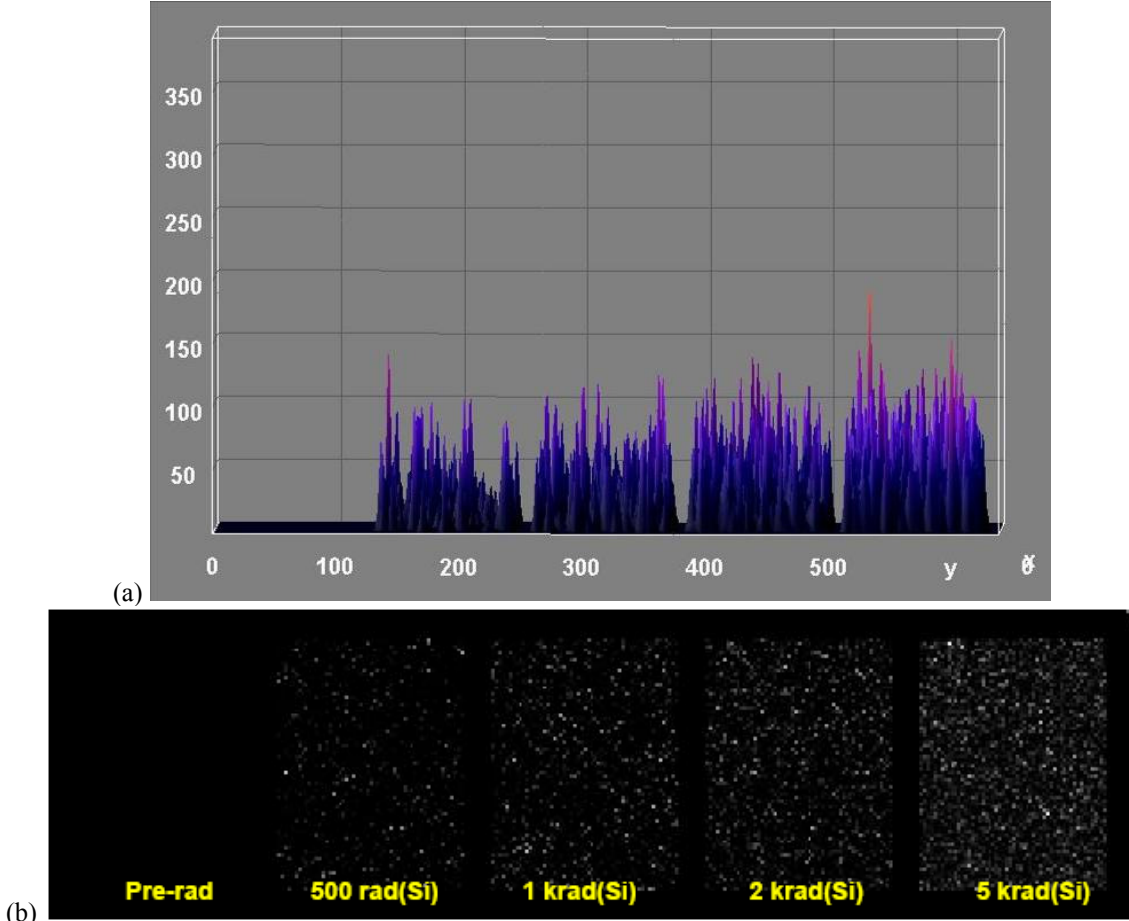| Irradiation Level	Pre-irradiation	500 rad(Si)	1 krad(Si)	2 krad(Si)	5 krad(Si)
Local DSNU (DN)	0.705	7.313	13.069	18.382	34.336

Fig. 12. Micron 5MPX Local DSNU. (a) 3D plot of rms dark rate values (in DN) for each 16x16 window of green1 pixels in the Micron 5MPX sensor. Irradiation levels increase from left to right, and pre-irradiation data are shown at the far left. (b) 2D surface plots for all five cases are shown below the 3D plot to further illustrate the variations across the array.

7.1.4 Photo-Response Non-Uniformity (PRNU)

Flat field images were used to determine the photo response non-uniformity (PRNU) of the Micron sensors. Sets of five frames collected at the same integration time were averaged, and a frame of pixel photo response rates was calculated using average frames for two different integration times. Rates were normalized, so that the average pixel response rate equaled 1. Our illumination system does not produce a perfectly uniform flat field, so a 6th order polynomial fit to the data was also needed to correct for the rolling off of illumination levels toward the edges of the array area.

A 226,576-pixel area of relatively flat illumination was used for 3MPX Micron PRNU calculations, and a 492,804-pixel area was used for the 5MPX. Table 5 shows the

standard deviation of pixel responses over the considered pixel area, relative to the mean response (where the mean response was normalized to 1). The standard deviations are expressed as a percentage of the average pixel response, and are given for each 3MPX and 5MPX sample tested. The pre-irradiation value (in parenthesis) corresponding to a particular test sample is shown together with the post-irradiation value. Both sensors have very small PRNU.

Table 5. Micron 3MPX and 5MPX PRNU*

Irradiation Level	500 rad(Si)	1 krad(Si)	2 krad(Si)	5 krad(Si)
Micron 3MPX PRNU σ over 226,576 pixels (percentage of average)	1.56 (1.40)**	2.14 (1.35)	2.39 (1.32)	3.38 (1.46)
Micron 5MPX PRNU σ over 492,804 pixels (percentage of average)	2.19 (1.45)	2.67 (1.48)	2.77 (1.45)	4.55 (1.68)

*The normalized photo responses used in our PRNU calculations have not been corrected for dark signal. The increase in calculated PRNU seen after irradiation may be driven by the known increases in post-irradiation DSNU.
**Pre-irradiation values are given in parenthesis.

The normalized photo responses used for our PRNU calculations have not been corrected for dark signal (this analysis is in progress). The increases in calculated PRNU may be driven by the known increases in post-irradiation DSNU. Nevertheless, the variation in photo response between pixels is still very small. Figure 13 shows the cumulative distribution function for the 5MPX sample that was irradiated to 5 krad(Si). This sample showed the largest spread in photo response among the examined pixels, with the maximum response being 1.91 times the average. However, 97% of the ½ million pixels included in the calculation were within only +/- 4% of the average pixel response.
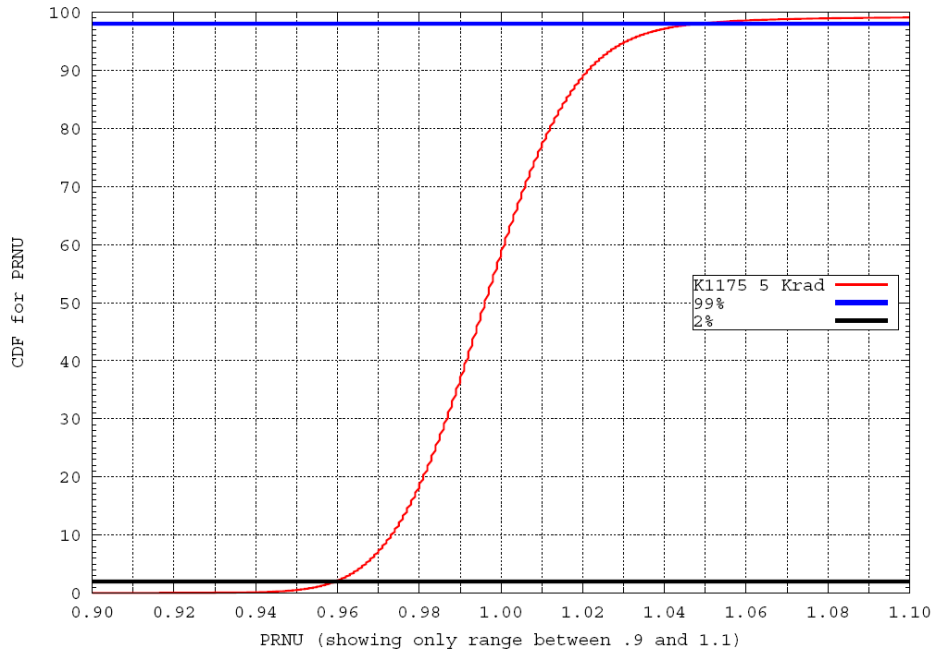

Fig. 13. Micron 5MPX cumulative distribution function for PRNU, showing that 97% of pixels have a relative photo response that is within +/- 4% of the average.

7.1.5 Pixel Noise

The average rms pixel noise was calculated from dark frame data (five frames were taken at each integration time) (Figures 14 and 15). As mentioned above, pixel noise under these conditions includes a combination of thermal dark current shot noise, output amplifier noise, on-chip electronic noise, and any uncorrected offset noise or pixel reset noise (also see Section 8.1.5 on the importance of random telegraph noise). Pixel noise was seen to increase with integration time, which may be due to the presence of increased amounts of thermally generated dark signal for longer integration times. Increased noise is also seen when data taken at the same integration time are compared for increasing levels of ionizing dose. Increases in noise with irradiation may be due to a combination of increased dark current and random telegraph noise.
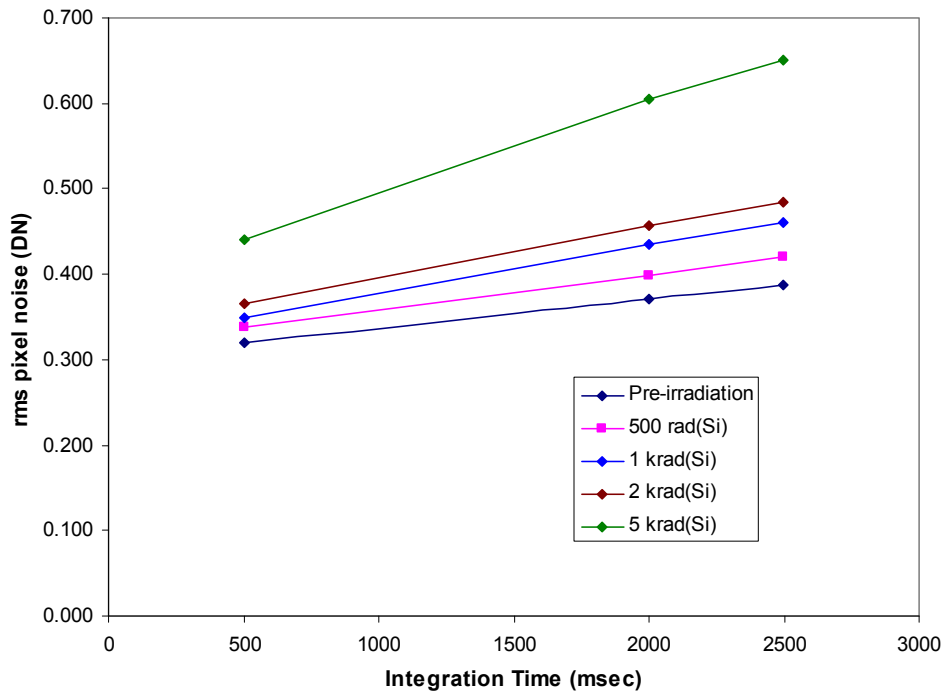

Fig. 14. Average rms pixel noise for the Micron 5MPX sensor. Increases in noise with irradiation may be due to a combination of noise from increased dark current and random telegraph noise.

Fig. 15. Average rms pixel noise for the Micron 3MPX sensor. Increases in noise with irradiation may be due to a combination of noise from increased dark current and random telegraph noise.
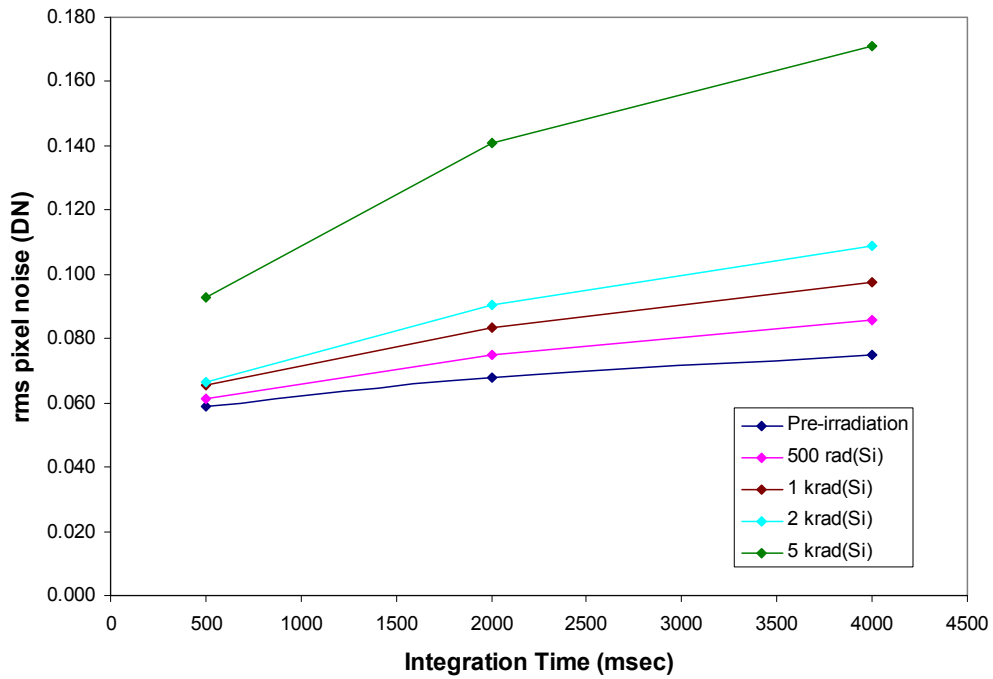
7.2 Bar Target Images (Auto)

Figure 16 compares a Micron 3MPX sensor image taken before irradiation to one taken after unbiased irradiation to 5 krad(Si) with 50-MeV protons. Image auto correction functions were enabled during the collection of both images, and the exposure time was 200 ms. Although hot pixels can be seen following irradiation, the overall image quality at 5 krad(Si) is still comparable to pre-rad performance.
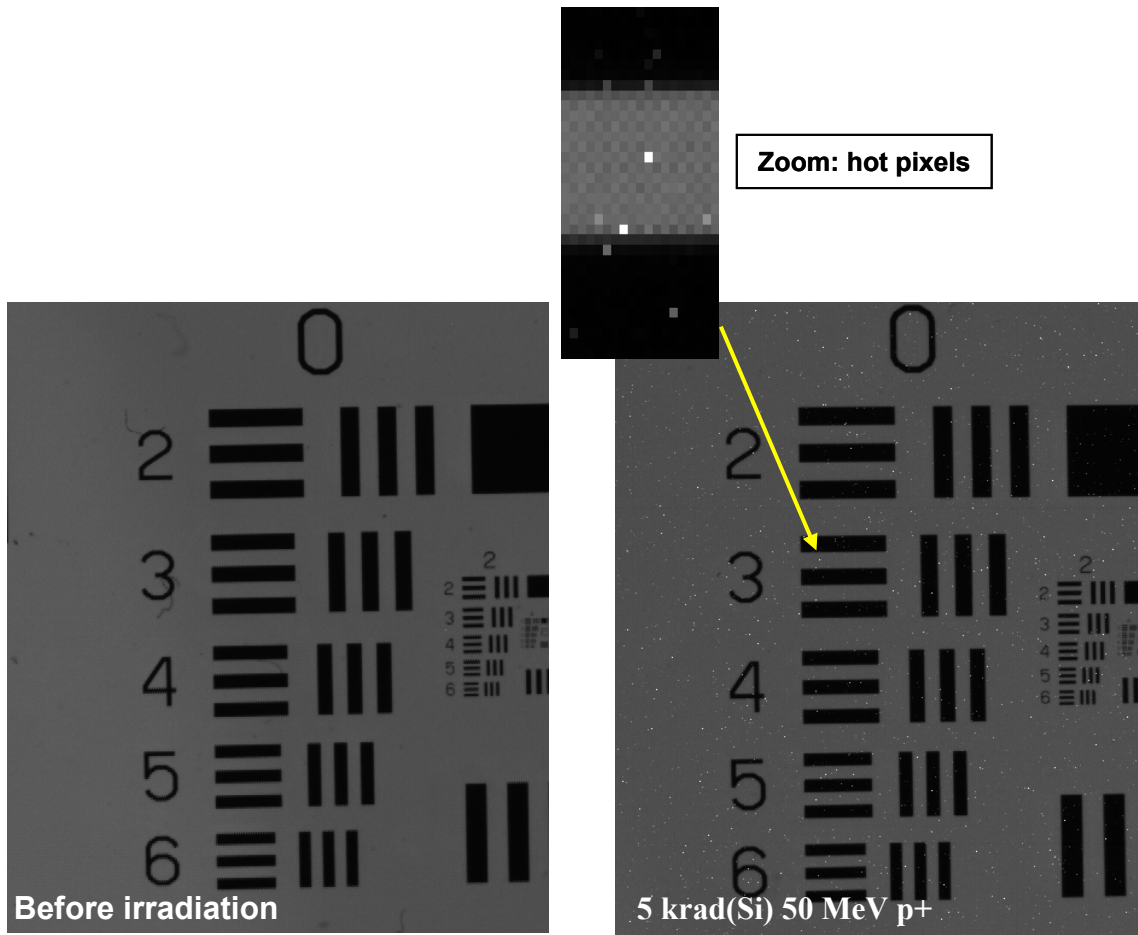
Fig. 16. Images collected with a Micron 3MPX sensor before and after irradiation to 5 krad(Si) with 50-MeV protons. Images were collected with auto correction functions enabled (the auto exposure time chosen by the sensor was ~200 ms in both cases). Image signal is approximately 350 DN/pixel.

Signal sizes of uncorrected hot pixels can be put into the context of an outreach camera application by comparing their magnitudes to that of a hypothetical scene. For example, if we consider a camera with a 3-mm diameter aperture and a 12-mm focal length, Earth's moon (as seen from a spacecraft ~9/10 of the way there) will create 8,187 signal electrons per pixel during a 1-ms exposure (a known quantum efficiency curve for another commercial CMOS sensor was assumed for this calculation). For the Micron 3MPX sensor, this corresponds to a signal of 315 DN per pixel. As can be seen in Figure 10, after irradiation to 5 krad(Si), approximately 0.03% of pixels have a dark rate that is at least 315 DN/second. With a 1-ms integration time, the dark signal contributed to the image would be only 0.3 DN per pixel, much less than the signal generated by the scene.

Comparison of manual and auto images is complex because more than one image correction variable is involved. Black-level calibration and the resultant digital offset correction would be expected to correct for the average dark signal rate increases seen after irradiation. However, analysis of this correction needs to be considered along with the analog offset corrections that are also made on a color-wise basis before the digital black-level correction takes place. *Analysis of the effect of sensor auto-calibrations on*

radiation degradation is ongoing, and will perhaps need to be supplemented with additional image collection of a colored scene to make a qualitative assessment of how well analog color offset corrections function following sample irradiation. With respect to hot pixels, the auto image correction features would not be expected to reduce the "black level" of hot pixels significantly, because their amplitudes are so much higher than the average pixel dark rates, as is observed in our data.

8.0   Omnivision Test Results

8.1   OV3630 Parametric Characterizations (Manual)

8.1.1   Dark Signal

Dark signal data were collected with integration times ranging from 50 ms to 400 ms, using a gain of 62 for all four color channels (blue, green1, red, green2). Five frames were taken at each integration time, and for each set of five frames, an average frame was calculated on a pixel-by-pixel basis. The mean dark rate was calculated for each pixel position by taking the difference of the average dark signal at two integration times, dividing by the difference in integration time, and normalizing for a gain of 1. Dark rate distribution data are shown in Figure 17.
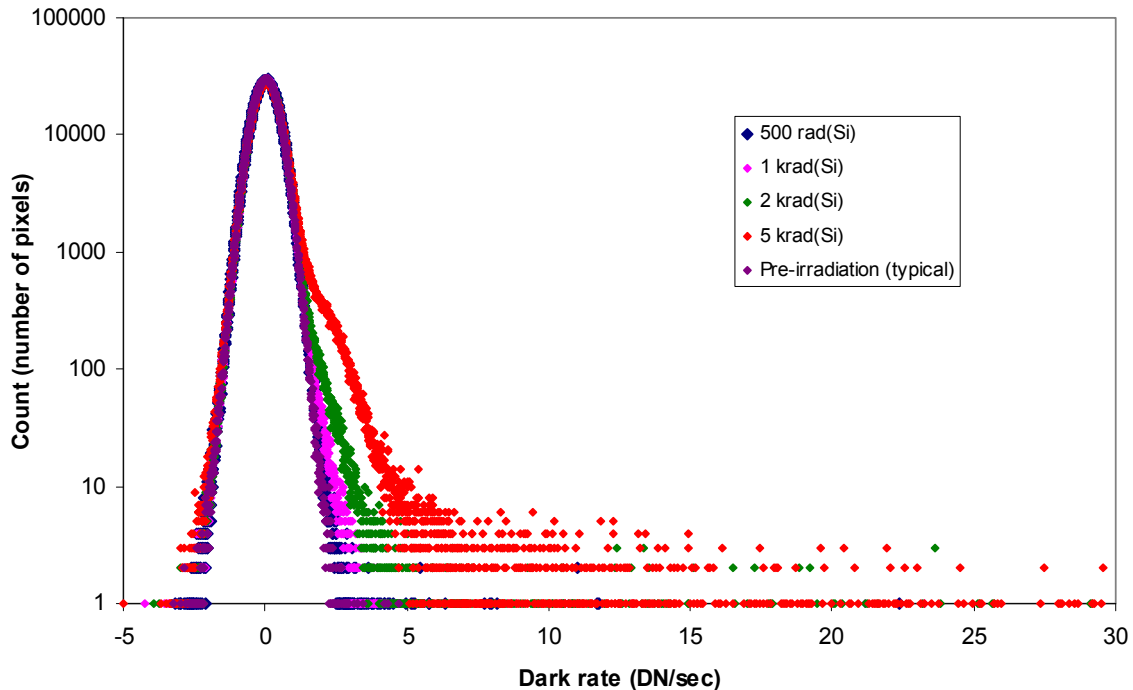

Fig. 17. Dark rate distributions for OV3630 samples irradiated unbiased with 50-MeV protons. A typical pre-irradiation dark rate distribution is included. Data were collected at ambient temperature, with on-chip image correction functions disabled.

Dark rate values ≤0 DN/s are due to pixel noise. The mean rms pixel noise over the 3Mpixel array is ~0.2 DN, which is comparable to average dark signal values at our 50–400 ms integration times. The peak of the distribution was relatively stable for all irradiation levels, indicating that dark rate increases were very small for most pixels. The tails of the distributions were seen to increase with proton fluence, however, due to an increasing number of hot pixels.

The mean dark rate over the entire image was calculated by averaging the mean dark rates of all the pixels in the array. Figure 18 shows mean dark rate as a function of ionizing dose, further illustrating the generally small increases in dark signal seen after our irradiations. The small susceptibility to radiation-induced dark rate increase is believed to be related to both the small 2.2 x 2.2 micron pixel area, and the small feature size of OmniVision CMOS CameraChip[TM] technologies (although information on the OV3630 feature size is not publically available, product briefs for OmniVision's 2.2 x 2.2 micron OV5620 5-Mpixel CameraChip[TM] advertise a 0.13-micron process technology [6]).
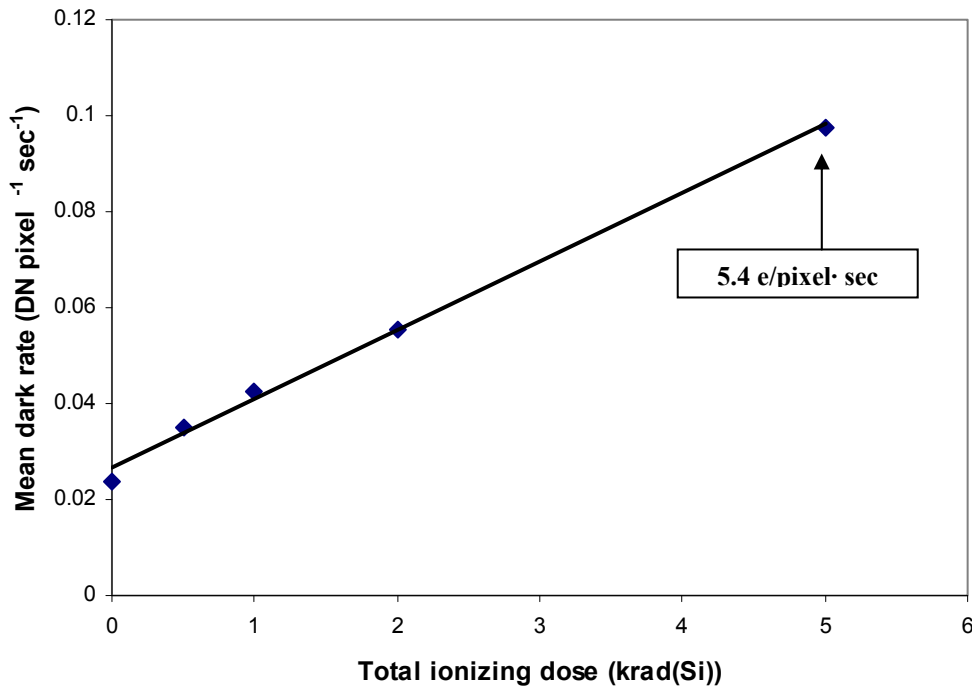

Fig. 18. Mean dark rate (at ambient temperature) vs. ionizing dose for OV3630 samples irradiated unbiased with 50-MeV protons. The pre-irradiation value is the average of our four test samples.

8.1.2 Dark Signal Non-Uniformity (DSNU)

Local DSNU was calculated for green1 pixels, using 16x16 windows, as was done for the Micron sensors (Table 6 and Figure 19). Although the OV3630 and the Micron 5MPX

have the same pixel pitch (2.2 x 2.2 µm), it is interesting that the OmniVision sensor has smaller DSNU. For example, at 5 krad(Si), Local DSNU is 31 electrons for the OV3630 and 86 electrons for the Micron 5MPX.

Table 6. OV3630 Local DSNU.
Local DSNU values (the average rms window values) for each irradiation level.

Irradiation Level	Pre-irradiation	500 rad(Si)	1 krad(Si)	2 krad(Si)	5 krad(Si)
Local DSNU (DN)	0.450	0.448	0.446	0.472	0.569
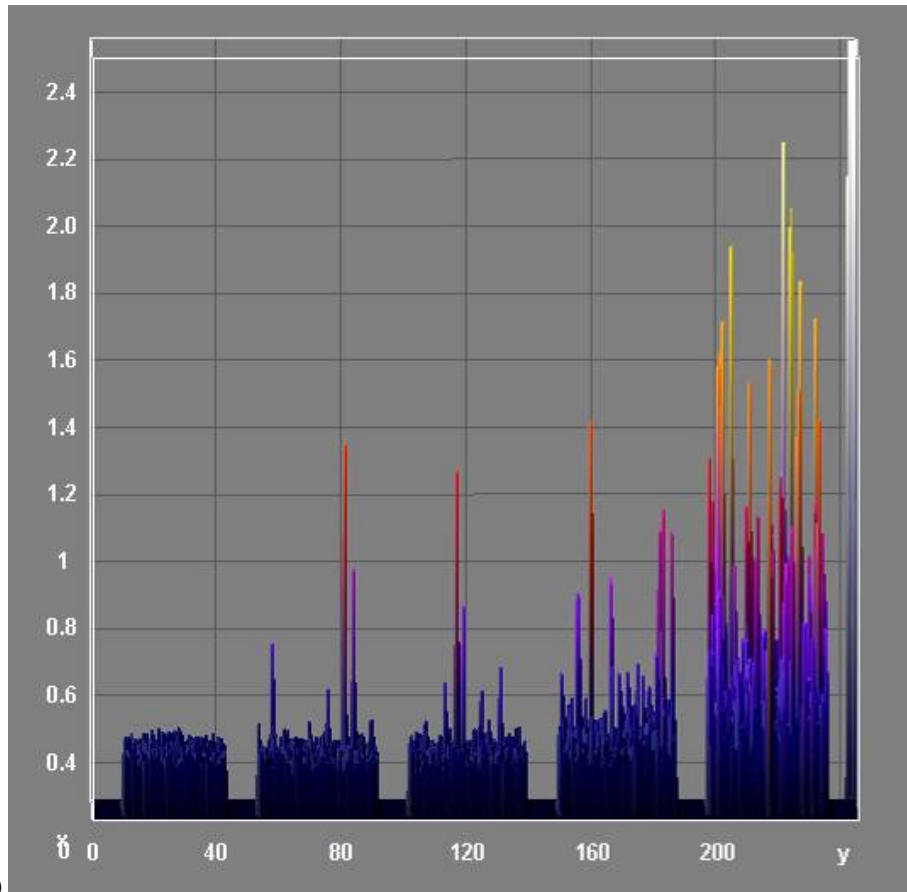
(a)
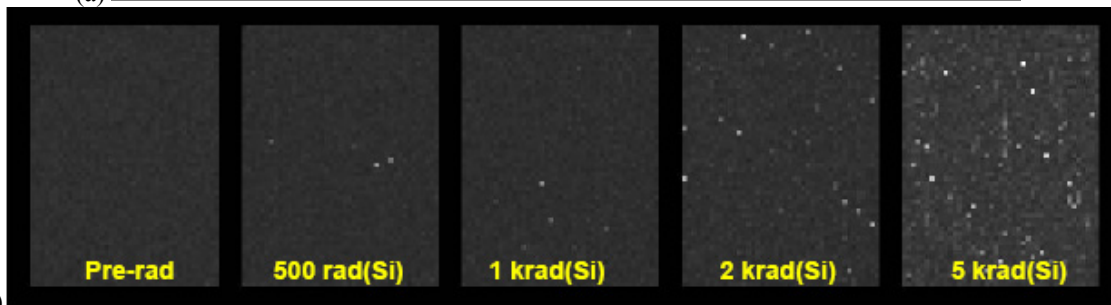
(b)

Fig. 19. OV3630 Local DSNU. (a) 3D plot of rms dark rate values (in DN) for each 16x16 window of green1 pixels in the OV3630. Irradiation levels increase from left to right, and pre-irradiation data are shown at the far left. (b) 2D surface plots for all five cases are shown below the 3D plot to further illustrate the variations across the array.

8.1.3 Photo-Response Non-Uniformity (PRNU)

PRNU was found to be very low for the OV3630. It was calculated as described in Section 7.1.4 (219,024 pixels were used in the OV3630 calculations), and was less than 1% at all radiation levels (Table 7).

Table 7. OV3630 PRNU*

Irradiation Level	500 rad(Si)	1 krad(Si)	2 krad(Si)	5 krad(Si)
OV3630 PRNU σ over 219,024 pixels (percentage of average)	0.92 (0.84)**	0.89 (0.81)	0.94 (0.84)	0.82 (0.88)

*The normalized photo responses used in our PRNU calculations have not been corrected for dark signal. The changes in calculated PRNU seen after irradiation may be driven by the known increases in post-irradiation DSNU.
**Pre-irradiation values are given in parenthesis.

8.1.4 Pixel Noise

Average rms pixel noise is shown in Figure 20. As with the Micron sensors, increases are seen with integration time and irradiation.
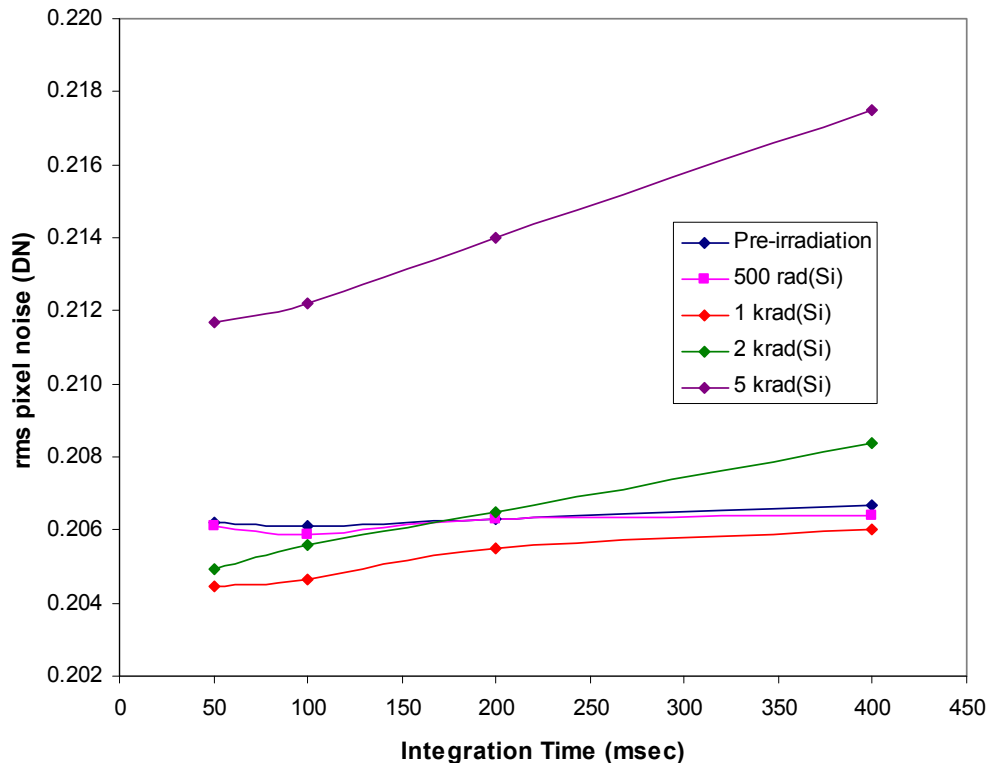

Fig. 20. Average rms pixel noise for the OV3630. Increases in noise with irradiation may be due to a combination of noise from increased dark current and random telegraph noise.

8.1.5   Flickering Hot Pixels

Several hot pixels were noticed to flicker "on" and "off" between successive collected dark frames. This signature is indicative of random telegraph signal (RTS), an effect where traps in the Si-SiO$_2$ interface of an individual pixel's source follower amplifier MOSFET capture and re-emit carriers (causing a variable current flow). RTS has previously been identified as a significant contributor to pixel noise in CMOS sensors [7]. This effect was observed in OV3630 samples both prior to and after irradiation, although the occurrence of these variable pixels was greatly increased for samples irradiated to our higher radiation levels. Because traps are created by ionization damage, a greater number of RTS pixels are expected in irradiated devices. RTS was also observed in the Micron 3MPX and 5MPX sensors.

Figure 21 shows sets of dark frames for a sample irradiated to 5 krad(Si) and an un-irradiated sample. RTS pixels can be seen to flicker "on" and "off" over the 3-second periods between successive images. An interesting feature of OV3630 RTS pixels (and OV3630 hot pixels in general) is that they often appear in pairs, or as "blinking eyes." The pixels in each pair are always the same color (e.g., both red), are always on the same row, have identical or near identical (within +/- 1DN) values, and are typically 2 to 6 pixels apart from each other. The reason for this topography is not known.
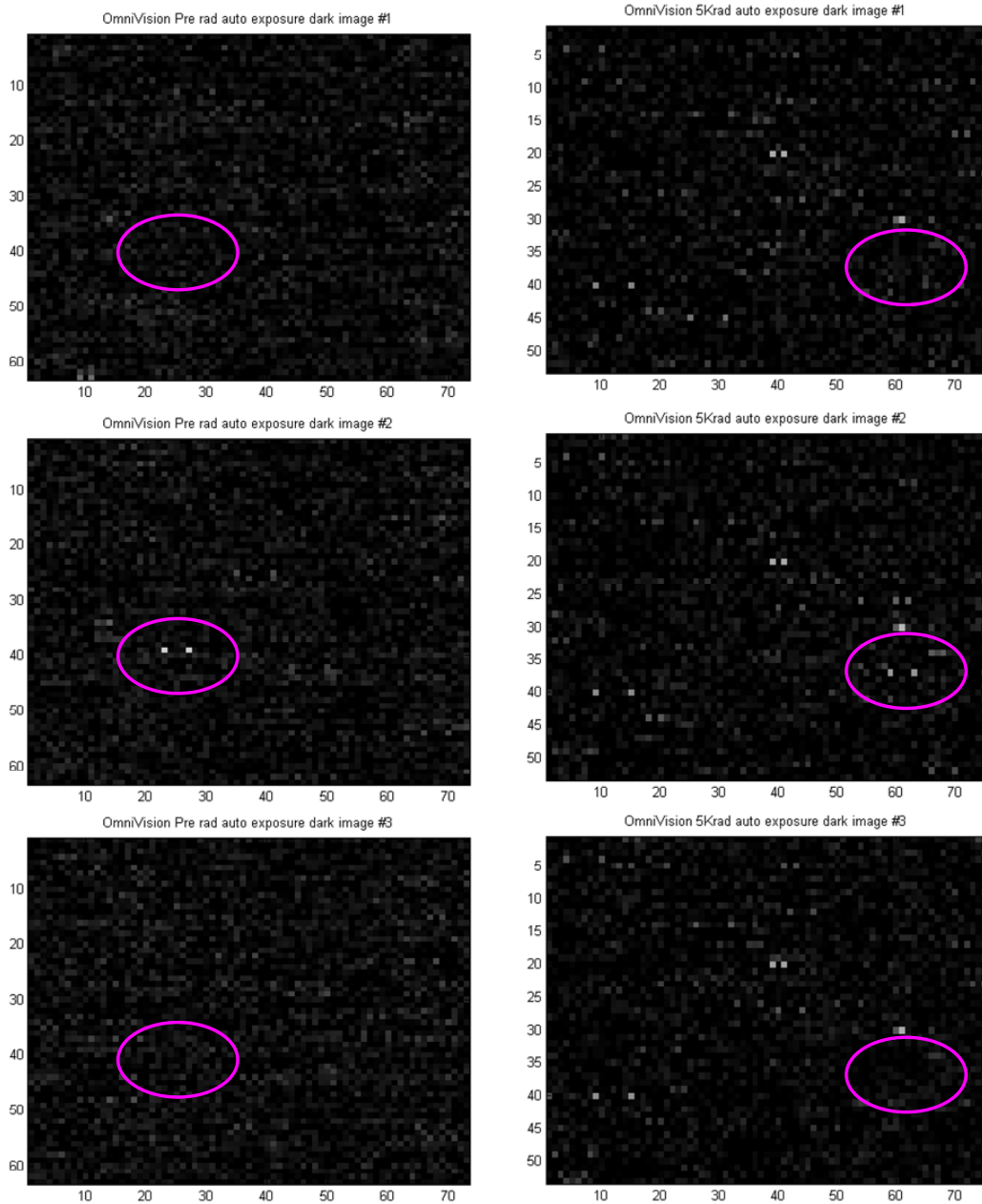
Fig. 21. Examples of pixels affected by random telegraph signal (RTS). *Left column*: Three dark frames taken ~3 seconds apart with an un-irradiated OV3630 sample. RTS pixel locations are indicated by the pink ellipse. Highlighted RTS pixels were "off" during the 1st and 3rd images, and "on" during the 2nd image. *Right column*: A similar set of three images for an OV3630 sample irradiated to 5 krad(Si). Two flickering RTS pixels are highlighted.

8.2 Bar Target Images (Auto)

Figure 22 shows images taken with OV3630 CameraChip™ image correction functions enabled. Images taken with the same sample before and after irradiation to 5 krad(Si) with 50-MeV protons are compared. Qualitatively, performance is very similar, although (as with the Micron devices) hot pixels in the 5 krad(Si) auto image are not corrected.
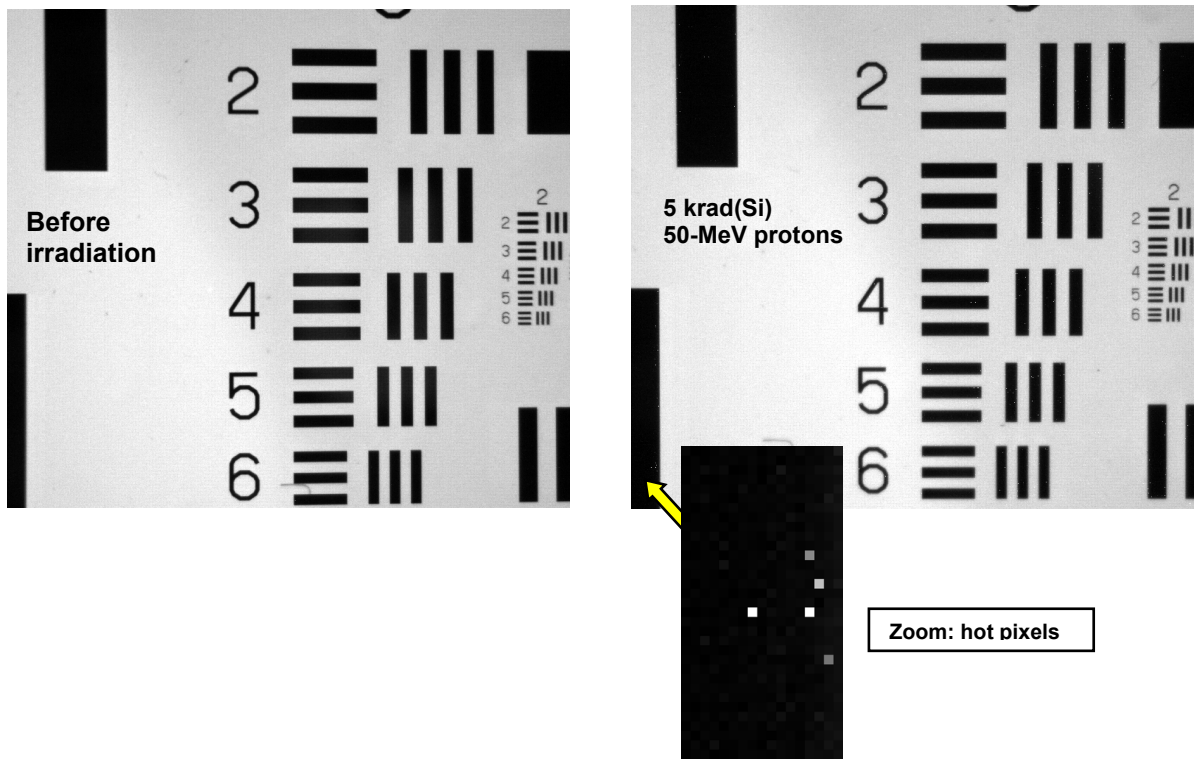
Fig. 22. Auto bar target images taken with OV CameraChip^{TM} image correction functions enabled. Imaging performance for a sample irradiated to 5 krad(Si) is qualitatively similar to that before irradiation, but increased numbers of hot pixels can be seen. Hot pixels are not corrected by the sensor's internal image correction functions. The integration time was 400 ms for both images.

9.0 Conclusions and Next Steps

Our selected Micron and OmniVision commercial CMOS sensors have all shown encouraging performance following unbiased proton irradiation to 5 krad(Si). Although the higher dark rate pixels ("hot pixels") created by such irradiations would not be correctable without using additional image correction strategies (such as the use of a shutter to allow the collection of dark frames for hot pixel mapping), the uncorrected presence of these pixels would not be expected to significantly impact image quality for an outreach or survey camera application.

Analysis of our February 2008 50-MeV proton test data is ongoing. The emphasis is on the impact that sensor auto-calibrations have on radiation degradation. Given the promising performance seen after unbiased proton irradiation, biased irradiations of our three sensor technologies are being planned for later in fiscal year 2008 (FY08), as well as additional unbiased irradiations to improve the statistics on our existing data.

10.0   References

[1]   Becker, H.N., Alexander, J.W., Thorbourn, D.O., and Konefat, E.H., "Commercial Sensor Survey Status Report," JPL Publication 08-8. February 2008.

[2]   Micron Technology, Inc. "MT9P031 1/2.5-inch, 5-Mp CMOS Image Sensor," Limited Data Sheet, © 2006. http://download.micron.com/pdf/product_brief/MT9P031_5100_PB.pdf. 13 July 2007.

[3]   Micron Technology, Inc. "MT9T031 1/2-inch, 3-Mp CMOS Image Sensor," Limited Data Sheet, © 2006. http://download.micron.com/pdf/product_brief/MT9T031_3100_PB.pdf. 13 July 2007.

[4]   OmniVision. "OV3630 3.2 MPixel product brief." http://www.ovt.com/data/parts/pdf/Brief3630V2.1.pdf, 13 July 2007.

[5]   OmniVision. "Support/Evaluation Modules." http://www.ovt.com/support/evalkits.asp. Accessed 25 March 2008.

[6]   OmniVision. "OV5620 5.17 MPixel product brief." http://www.ovt.com/data/parts/pdf/Brief5620V4.2.pdf. 13 July 2007.

[7]   Janesick, J., et al., "Fundamental performance differences between CMOS and CCD imagers; Part 1," *Proc. of SPIE*, Vol. 6276, High Energy, Optical, and Infrared Detectors for Astronomy II. 15 June 2006.